# CHARACTERIZATION OF ALTERNATING POLYFLUORENE GREEN-6 AND [6,6]-PHENYL $C_{61}$-BUTYRIC ACID METHYL ESTER(PCBM) BASED BULK HETEROJUNCTION SOLAR CELL

A Thesis Submitted to the School of Graduate Studies
Addis Ababa University

In Partial Fulfilment of the Requirements for the
Degree of Master of Science in Physics

By

***Tesfaye Mamuye***

Addis Ababa, Ethiopia

July 2006

**ADDIS ABABA UNIVERSITY**
**FACULTY OF SCIENCE**
**DEPARTMENT OF PHYSICS**

The undersigned hereby certify that they have read and recommend to the Faculty of Science School of Graduate Studies for acceptance a thesis entitled "**Characterization of alternating polyfluorene green-6 and [6,6]-phenyl $C_{61}$-butyric acid methyl ester(PCBM) based bulk heterojunction solar cell** " by ***Tesfaye Mamuye*** in partial fulfillment of the requirements for the degree of **Master of Science in Physics**.

Dated: July 2006

| Name | Signature |
|---|---|
| Dr. Genene Tessema, Advisor | _____ |
| Dr. Shimeles Admassie, Examiner | _____ |
| Dr. Mebratu G/Mariam, Examiner | _____ |

***This Work is Dedicated to***
***My Mother***

## Acknowledgements

I have a high debt of gratitude to my advisor, Dr. Genene Tessema, for introducing me to the field of conjugated polymer, excellent guidance, encouragement, and material support. The working environment he has created with necessary journals and materials are greatly acknowledged.

Special thanks to Dr. Wondimagegn Mammo, from department of chemistry, for providing me with the polymer:-APFO green-6. I also sincerely thank Dr. Teketel Yohannis, Dr. Shimelis Adimassie, Ato Assefa Sergawie, and Ato Ashenafi Asrat for their encouragement and constructive suggestion. I am thankful to all my friends and colleagues who showed co-operation in one way or another way to the success of this work.

Last, but not least, I thank the physics department community and the instructors for their help in one way or another for my success.

***Tesfaye Mamuye***
**July,** 2006
**Addis Ababa.**

## Abstract

Photovoltaic device based on blend of alternating polyfluorene green-6 (APFO Green-6) and [6,6]-phenyl $C_{61}$-butyric acid methyl ester(PCBM) in a sandwich structure of ITO/PEDOT-PSS/APFO Green-6:PCBM/Al was fabricated. The device was characterized by analyzing the current density-voltage measurements under dark and illumination as well as by impedance spectroscopy. The observed J-V curve under dark agree well with the trap-controlled space charge limited transport theory. The main solar cell parameters recorded at room temperature under 80mA/cm$^2$ white light intensity are: $V_{OC}$ = 547mV, $J_{SC}$ = 0.314mA/cm$^2$, with power conversion efficiency 0.107 %, and fill factor, of 0.5. The complex impedance analysis exhibits a bias voltage dependent whose Cole-Cole plot is a single semicircle. This is modelled by one parallel RC circuit, usually obtained from metal-semiconductor(MS) device.

# Contents

# List of Figures

# List of Tables

# Chapter 1

## 1.1 Introduction

polymers with an extended $\pi$-electron system show the properties of electrical conductivity [1]. This effect was first discovered in 1977 for polyaccetylene by H. Shirakawa, A. MacDiarmid and A. Heeger [2,3]. The science and application of conjugated polymers has made rapid progress since that time and, this discovery was honored by awarding the Noble prices in 2000 for the three discoverers.

In the intrinsic state; the conjugated polymers are either or insulator or semiconductors. The conductivity of such polymers can tuned by doping; from nearly insulating property in un-doped state to metallic like conductivity for highly doped conjugated polymers. Doping conjugated polymers are either oxidation or reduction. Their semiconducting behavior makes them active components in electrical and optical devices. Unlike the conventional inorganic semiconductor devices, the polymer based devices are easy to fabricate at a very low cost. There are numerous reports on the use of conducting polymers in electrical and optical devices such as photovoltaic devices [4], transistor [5] and polymeric light emitting diode [6].

Renewable energy sources such as wind, water and solar energy, are abundant in nature and can be utilized without harmful effect to the environment. One of the

promising renewable energy source is the the energy from the sun. An enormous amount of solar energy is radiated toward the earth continuously. The conversion of solar energy from the sun to electricity can be made in a device called solar cells, also known as photovoltaic (PV) cells. Harvesting solar energy directly from the sun using photovoltaic technology is widely recognized as an essential component of future global energy production. Provided that the photovoltaic device can be made at a cost comparative with the cost of conventional energy source ( i.e., oil, coal ).

Solar cells made from inorganic semi-conductors have been studied since 1950s when Chapion et al. reported a solar cell energy conversion efficiency of 6 % [7] for single-crystalline silicon solar cells. Since then, the efficiency has reached 24 % for crystalline silicon solar cell [8]. At present, crystalline silicon solar cells are by far most dominant photovoltaic devices used that accounts for more than 85 % of the market [9]. However, the semiconductor photovoltaic still account for less than 0.1 % of the total world energy production. One of the major obstacle for marketing of inorganic photovoltaic cells is the high production cost for silicon based technology. Therefore, to ensure a sustainable technology for solar cells, the development of new materials and devices structures are required.

Development of material engineering in nano scale has generated new photovoltaic materials and system that could potentially lead to the realization of low cost solar cells. A promising approach towards low production cost of photovoltaic device is fabrication of solar cells based on organic materials. Solar cells based on these materials are called organic solar cells.

The first generation of organic solar cells was based on single layer sandwich structure between two metal electrodes of different work function [10,11]. The difference

in work function provides an electric field which separated and drives charge carriers. This electric field is seldom sufficient to breakup the photo-generated excitons. Instead, the exciton diffuse within the organic layer until it reaches a contact, where it may be break up to supply separate charges, or recombine. Since exciton diffusion lengths are short, typically about 10nm [12-14], exciton diffusion limits the charge carrier generation in such devices. Single layer solar cells of this type delivered power conversion efficiencies of less than 0.1 %[15].

Most of the developments that have improved performance of organic PV devices are based on donor-acceptor heterojunction. Normally, electric field will result at interface between two materials having different work function. These local electric field are strong and may break up photo-generated excitons provided that the difference in the potential energy are larger than the exciton binding energy. In a bilayer devices, the organic donor-acceptor interface separates excitons much more efficiently than the organic-metal interface in a single layer device.

The discovery of ultrafast charge transfer in conjugated polymer/fullerene composites by Sariciftci et al. in 1992 [14] was a crucial milestone in the field of polymer solar cells. The high asymmetry between forward and backward electron transfer [16] allows the use of the cell architectures with one photoactive composite layer instead donor-acceptor bilayer devices. The advantage of the blend is an increased donor-acceptor interface and shorted the distance for exciton diffusion to reach it. In 2001 Shaheen et al.[17] obtained the first truly promising result for MDMO-PPV blended with PCBM [1:4 wt %] and optimizing the nanoscale morphology of the thin film yielding and a power conversion efficience of 2.5 %. Recently, power conversion efficiency of $> 3.5$ % have been achieved for polymer:fullerene bulk-heterojunction solar cells using poythiphene derivatives [such as regioregular P3HT ] [18-21].

The objective of this experimental research work is to characterize polymer based photovoltaic device whose active layer composed of alternating polyfluorene green-6 (APFO Green-6) and [6,6]-phenyl $C_{61}$-butyric acid methyl ester(PCBM). Devices was characterized by I-V measurements under dark and illumination as well as by impedance spectroscopy. We used space charge limited conduction theory to interpret I-V curve under dark. Photovoltaic parameters such as short-circuit photocurrent density $J_{SC}$, open circuit voltage $V_{OC}$, fill factor (FF) and power conversion efficiency $\eta$ were calculated from I-V under illumination measurements.

# Chapter 2

# Basic properties of conjugated polymers

## 2.1 Bonding

The formation of a covalent bond involves the sharing of two electron, i.e.,the pair that can be accommodated in the bonding molecular orbital. Two different geometries are possible which in turn gives two types of bonds. The first one is a bond that is cylindrically symmetric around an axis joining the two nuclei is called sigma($\sigma$) bond as shown in Fig. 2.1. The other bond is the pi($\pi$) bond that is formed by side chain overlap of parallel p orbital see Fig. 2.2

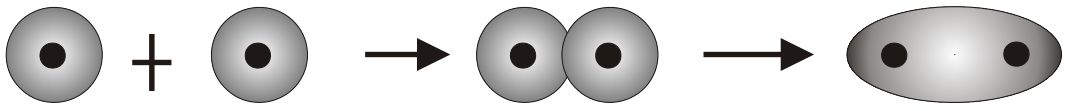

Figure 2.1: Cylindrically symmetric $\sigma$-bonding of hydrogen molecule.

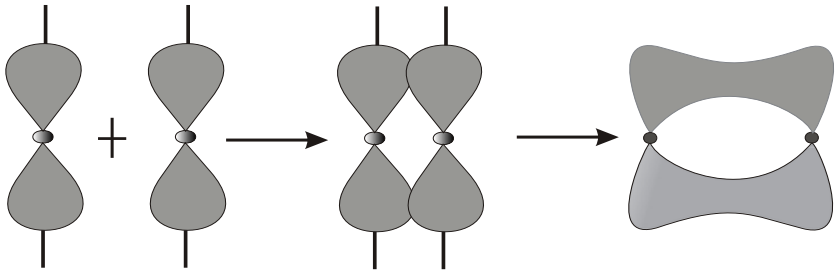

Figure 2.2: Two parallel orbitals overlap to form a $\pi$- bonding MO

Generally, the $\sigma$-electrons are responsible for the strong covalent bond and are localized between the two bonded nuclei. The $\pi$-electrons are also involved in chemical bonding, but they tend to form weaker and less localized bonds since there are no electrons density between the two nuclei, it is all concentrated into electrons clouds above and below the plane of the bond.

## 2.2 Electrical and structural properties of conjugated polymers

The ground state of electronic configuration of carbon atom is $1s^2\ 2s^2\ 2p_x^1\ 2p_y^1\ 2p_z^0$ . One of the 2s electrons jumps to the empty p-orbital when the atomic carbon is in its excited state, thereby changing the atomic orbital configuration to $1s^2\ 2s^1\ 2p_x^1\ 2p_y^1\ 2p_z^1$. Therefore, the molecular orbital of carbon are described as a hybrids formed by $2s^1\ 2p_x^1\ 2p_y^1\ 2p_z^1$ atomic orbitals.

In $\sigma$-bonded polymers, the C-atoms are $sp^3$ hybridized as in the case of polyethylene, which is the prototype of the entire class of convectional polymers [22]. In such non-conjugated polymers, the electronic structure of the chain of atom ( or chemical group ), which comprises the backbone of macromolecule, consists of only $\sigma$-bonds.

However, in conjugated polymers such as polyacetylene, which is often used as a model compound for describing the electronic properties of conjugated polymers, three of the four atomic orbital of the C-atoms, with one 2s character ( $2s^1$ ) and two 2p character ( $2p_x^1$ $2p_y^1$ ) will form three $sp^2$ hybridized orbital; two of the three orbital will form $\sigma$-bond on either side with the other C-atoms and one with hydrogen atom. Thus, polyacetylene essentially comprise a backbone of $sp^2$ hybridized C-atoms linearly attached. The electron in the $p_z$ orbital of each $sp^2$ hybridized C-atom form $\pi$- bonds with the neighboring $p_z$ electron in a linear chain of $sp^2$ hybridized C-atoms. The $\pi$-bonds allow electrons to move easily; such electrons are delocalized [22].

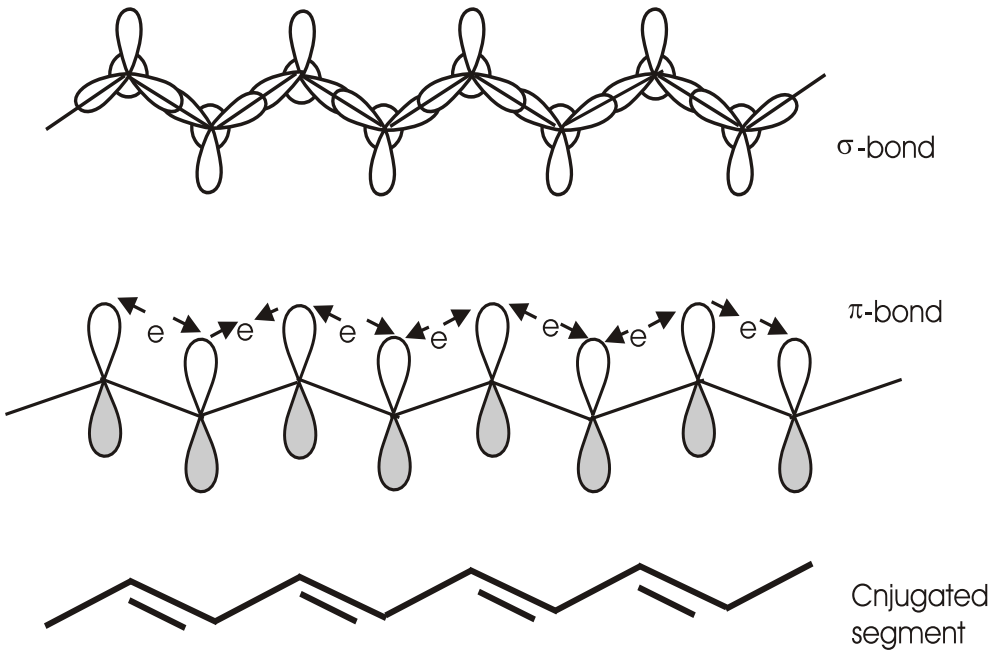


Figure 2.3: Formation of $sp^2$ hybridized orbitals of polyacetylene resulting in strong $\sigma$-bonds along a conjugated segment and $\pi$-bonds resulting from $p_z$ orbitals located orthogonally with respect to the plane of $\sigma$-bonds.

If the bond length between adjacent carbon atoms in polyacetylene chain is equidistant (undimerized i.e. all carbon-carbon bond lengths are equal and the $p_z$

electrons are delocalized over the whole system see Fig. 2.4 (a), then the unit cell should consist of one carbon atom and one $\pi$-electron. This implies that polyacetylene would act as a metal, because one electron per unit cell would lead to a partially filled band [23].

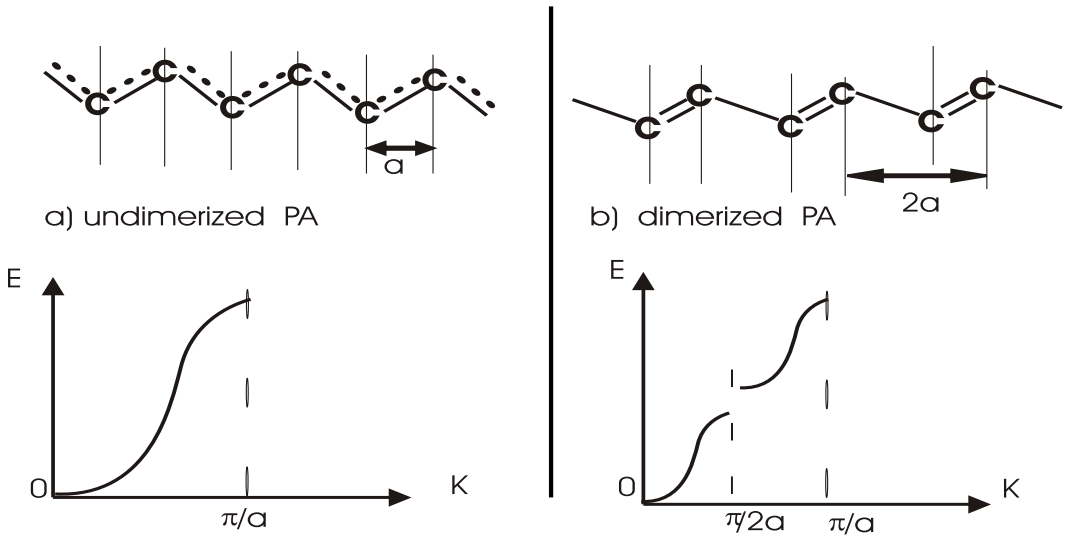


Figure 2.4: The formation of a band gap at the border of the first Brilloun zone.(a) equal length of the bond will yield a metal behavior.(b) alternating single and double bonds due to Peierls distortion, will render semiconducting behavior.

However, after the dimerization ( Peierls distortion is a disorder to order phase transition in the electronic system), an alternating single-and double bonds ( $\sigma - bond$ and $\sigma + \pi - bonds$ ) structure appears. This bond alternation corresponds to a pair-wise arrangement of spare electrons thereby pairing the CH radical [24]. Such a pairing of CH groups distorts the regular array of lattice and double the elementary cell of one dimensional crystal from **a** to **2a** as shown in Fig. 2.4 (b). Doubling of an elementary crystal cell in real space correspond to reducing the Brillouin zone by half in a reciprocal space. This introduce a discontinuity in dispersion relation. That means a gap at the boundary of the first Brillouin zone will open up ( see Fig. 2.4,b )

and thus create a band gap characteristics of semiconductors [25,26]. This also called Peierls gap after [26] the physicist R.E. Peierls, who first showed that one- dimensional metal having equidistant bond length would be energetically unstable and the system would be found to be in a dimerized state. Thus, because of Peierls distortion, adjacent CH group move towards each other, forming alternating single and double bond, thereby lowering the electronic energy by opening energy gap at the Fermi level.

Polymers have an alternating single and double bonds producing $\pi$ molecular orbital (MO) on a $\sigma$ framework. These $\pi$ MOs i.e., ($\pi$) bonding and ($\pi^*$) anti-bonding converge into two bands with which the MO spacing is so small that it can be regarded as a continues rather than discrete energy levels. The spacing between the two energy i.e., between the highest occupied molecular orbital( HOMO ) and the lowest unoccupied molecular orbital( LUMO ) is called the band gap. The HOMO-LUMO level is analogous to the valence band and conduction band in inorganic materials. Figure 2.5 show band formation in poly [paraphenylene vinylene] [PPV].

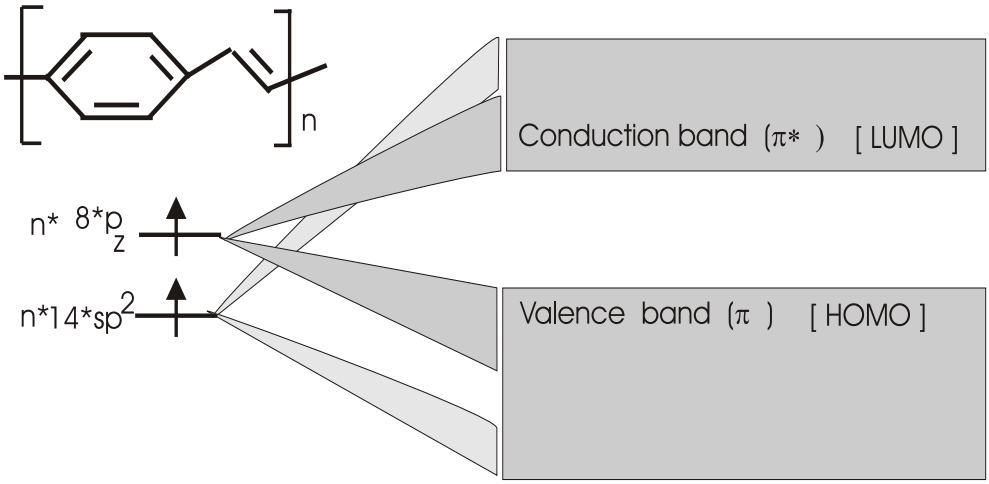


Figure 2.5: The formation of band in PPV.

In fact, the conjugated structure is the origin of the interesting electronic properties of conducting polymers. The $\pi$-electrons fills the highest occupied states below the Fermi energy, whereas the $\sigma$-bonds lies further down. Therefore, the $\pi$-electrons becomes the most important with respect to the electronic properties [27]: light absorption and emission, and charge generation and transport. The most common types of polymer chain are given blow.

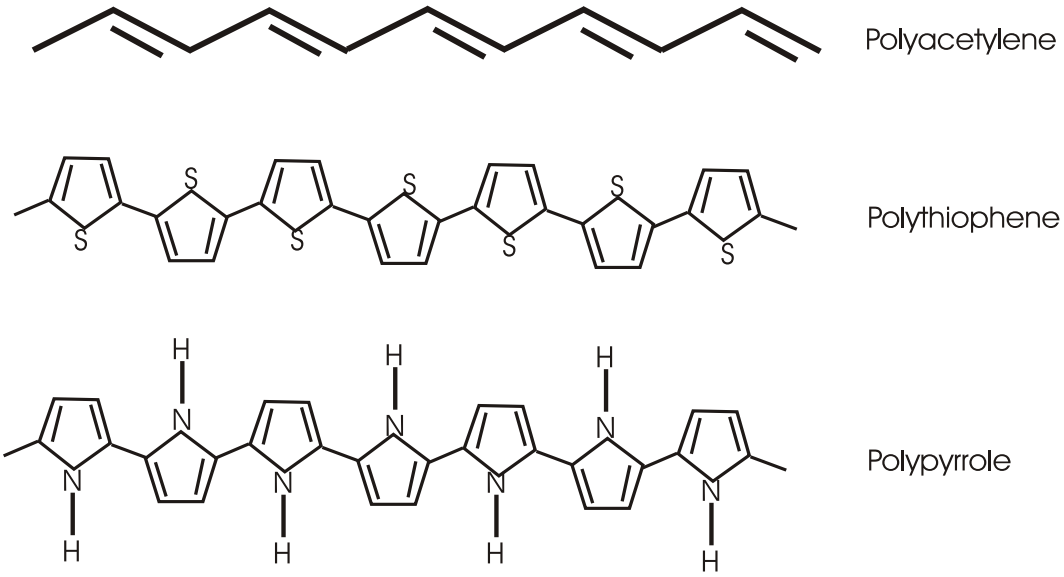


Figure 2.6: Basic chemical structure of some of the conjugated polymers.

## 2.3 Elementary excitation

### 2.3.1 soliton

The alternating single and double bond arrangement in trans-polyacetylene (PA) creates two possible degenerate ground states with the same energy as shown in Fig. 2.7.

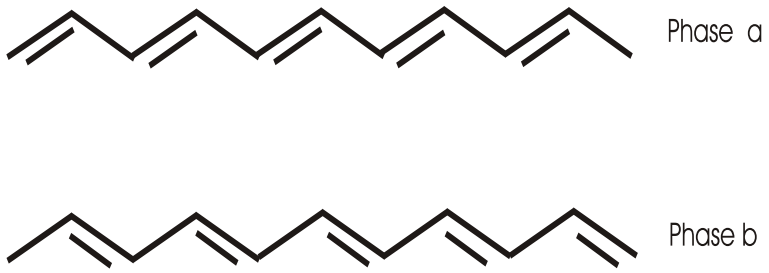


Figure 2.7: Ground state of degeneracy of dimerized trans-polyacetylene.The ground state energy of phase **a** is the same as that of phase **b**.

Let us imagine that undimerized trans-polyacetylene chain undergoes dimerization i.e., Peierls transition. Assume that the dimerization starts simultaneously at both end of trans polyacetylene chain and propagated to the center. When they meet [25], there is a 50 per cent probability of a misfit ( two single bond meet ).

Figure 2.8: A domain wall ( soliton ) separating a trans-polyacetylene chain into domains similar to phase **a** and phase **b** in figure 2.7

This is a domain wall (soliton) separating two iso-energetic region in opposite sense of bond alterations. In chemical language, there is a non-bonding orbital, in the neutral, uncharged chain is occupied by a single electron that we can think of as given by the 2p orbital of the carbon atom without double bond on. This excitation of the chain has a spin 1/2 and charge zero state: in other word a free radical.

Over the soliton extension, the bond alternation and the Peierls gap vanishes.

In other words solitons are extension that tend to violet the Peierls transition and, therefore, there is no gap. Soliton is a structural defect associated with localized electronic state whose energy lie in the middle of the band gap [28].

In addition to the intrinsic generation of soliton during synthesis or dimerization, doping is another mechanism of generation of soliton. Doping of conjugated polymers is a chemical redox reaction. As a result of charge transfer, there are three possible solitonic charges namely, mid-gap state with the charge +e, 0, or -e charge. The schematic band diagram is shown Fig. 2.9.

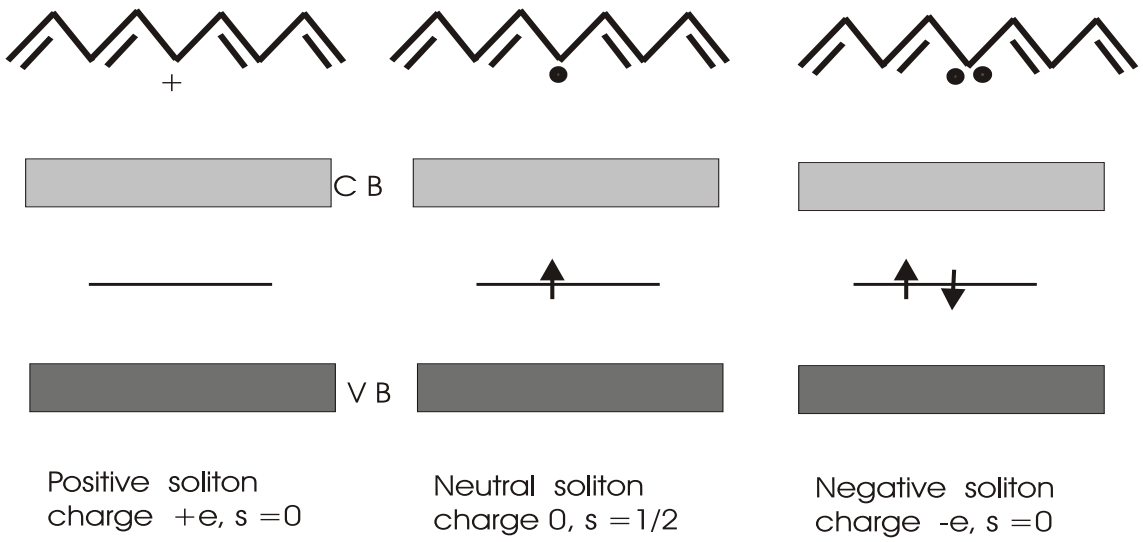


Figure 2.9: Schematics of the band diagram of polyacetylene with solitons. Charged solitons do not have spin while neutral solitons have spin s=1/2.

### 2.3.2 Polaron and Bipolaron

Trans-polyacetylene has a degenerate ground state. However, most other conjugated polymers have non degenerate ground state i.e., upon bond alternation the ground state energy will change. The aromatic form, for example, a polythiophene

Fig. 2.10(a) demonstrate a lower ground state energy compered to its quinoidal Fig. 2.10(b). In trans-polyacetylene, it does not matter wether the double bond is on the negative or the positive slope. However, in polythiophene, breaking the conjugation at the misfit lead to a transition from the aromatic ( two bonds in a ring and a single bond between the ring ) to a qoiniodal state ( with only one double bond in a ring and double bond separating the ring ).

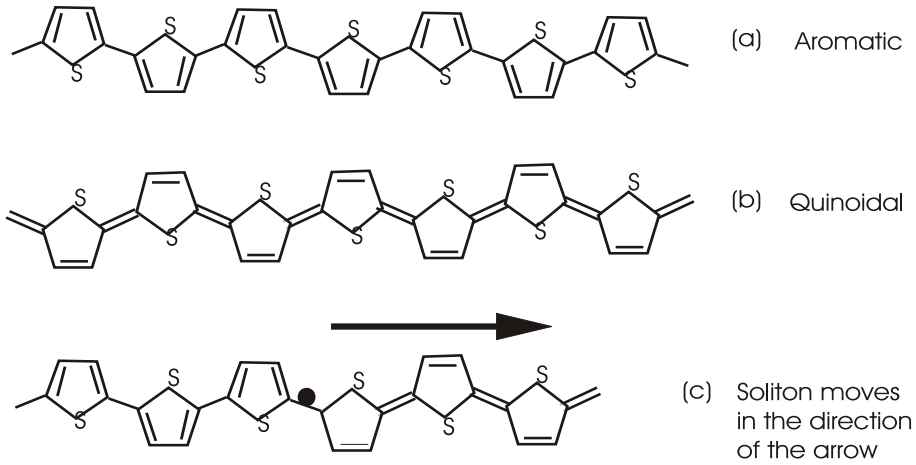


Figure 2.10: Aromatic (a) and quinoidal (b) in polythiophene ,and (c) soliton site in polythiophene.

Contrary to soliton in polyacetylene, which are more stable and can be positioned anywhere in the chain, solitons in non-degenerate polymers are energetically unstable. They move along the chain, thereby changing the high energy quinoidal rings [25] in to low energy aromatic rings see Fig. 2.10(c). If defects in non-degenerate ground state polymers are to be stable bound double defects must be created. This double defect is called **polaron** if it is singly charged, Fig. 2.11(a), otherwise if it is doubly charged it is called **bipolaron** Fig. 2.11(b)

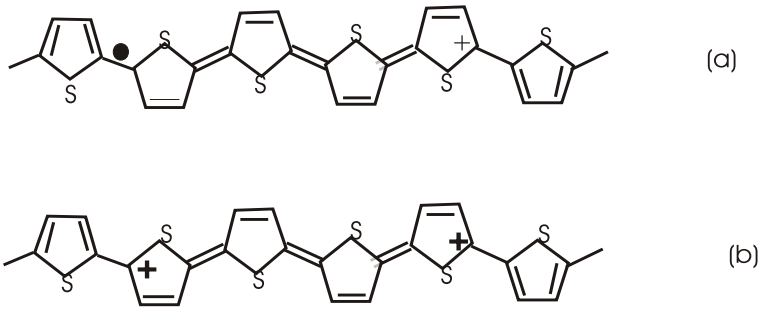


Figure 2.11: A polaron (a) and bipolaron (b) in polythiophene.

The two kinks in a polaron (and a bipolaron ) give rise to two interacting states which are energetically separated in the gap, unlike mid-gap of soliton. The schematics of the energy band diagram for both polaron and bipolaron are depicted in Fig. 2.12.

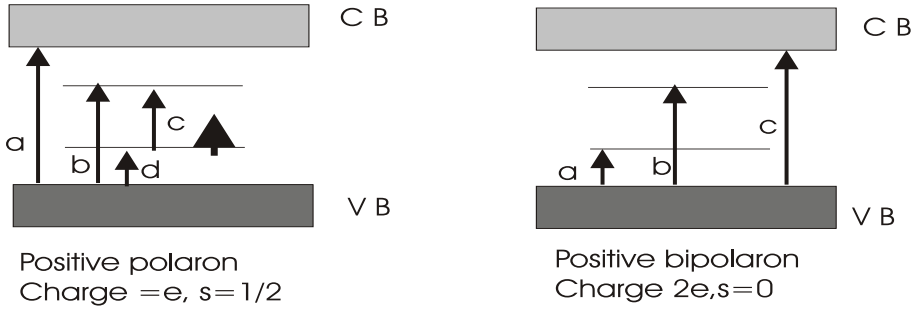


Figure 2.12: The band diagram of a hole polaron (left) and a hole bipolaron (right) with respective optical transition.

As depicted in Fig. 2.12, the optical signature of a polaron is characterized by two states in the gap. The formation of the states is attributed to the interaction between the mid-gap state of soliton components of the polaron, or bipolaron. Optical

absorption spectroscopy has evidenced the existence of two gap states. For the hole polaron, there are four possible transitions, three of which ( b, c, d in Fig. 2.12 left ) are sub gap transitions induced upon doping. For the hole bipolaron, the two gap states are empty, and therefore, transition from the lower state to the upper state is not observable. This leaves only three possible optical transitions, namely, 'a'= transition from VB to the lower state, 'b'= transition from VB to the upper state, and 'c'= the inter-band transition ( Fig. 2.12 right ).

## 2.4 Charge Transport in Conjugated polymers

Conductivity of materials depend on temperature. For pure metals conductivity increases with decreasing temperature because of lattice vibrations, which act as obstacles for the charge carriers, freeze out when cooling the metal. On contrary, cooling of an intrinsic crystalline semiconductors decreases its electrical conductivity. This attributed to the fact that cooling freeze out not only lattice vibration but also charge carriers. In amorphous semiconductors there is no continues carriers motion at all. This carriers are localized, and can only move with the help of lattice vibrations consequently the electrical conductivity increases with increasing temperature, but it doesn't increase exponentially as crystalline semiconductors [29].

In conducting polymers the conductivity is due to the presence of solitons, polarons and bipolarons, which are formed by self localization of carriers introduced in to $\pi$-electronic systems through doping [30]. These solitons, polarons and bipolarons are not truly mobile [31], coasting along one end of an infinite polymers chain to another, as in the idealized one-dimensional conduction model. Rather, they are localized by features such as defects or discontinuities in the extended conjugation.

The temperature dependence of the conductivity of conducting polymers are appears to be quite different at different doping levels [31]. Lightly doped or un-doped conducting polymers show strong temperature dependence of the conductivity. The room temperature conductivity is low and its conductivity vanishes at 0K. The charge transport is described to occur though hoping between localized solitonic, polaronic or bipolaronic states. Accordingly, the Mott's variable range hopping( VRH ) theory [32], which was proposed to explain the conductivity of amorphous semiconductor, is applied for un-doped or lightly doped conjugated polymers. The VRH theory assumes that the localization of the states is weak, allowing electrons to jump further away than to the nearest available site, thereby making it possible for them to find a states with lower energy than the nearest neighbor states. The term variable range describe this flexibility in finding appropriate site. When temperature increases, the number of available states rises and the average hoping distance decreases, resulting in higher conductivity. The temperature dependence of the electrical conductivity is described by

$$\sigma = \sigma_o exp\left[-\left(\frac{T_o}{T}\right)^{\gamma}\right] \tag{2.1}$$

Where $\sigma_o$ and $T_o$ are fitting parameters which are generally experimentally determined, and $\gamma$ depends on the dimensionality d of the hopping process and is given by

$$\gamma = \frac{1}{1+d} \tag{2.2}$$

In three dimensional hopping d=3 and $\gamma$ =4 and hence

$$\sigma = \sigma_o exp\left[-\left(\frac{T_o}{T}\right)^{1/4}\right] \tag{2.3}$$

The model has been shown to be appropriate for polyacetylene [33], and polypyrole [34].

Detail experiments have shown that the charge transport in highly doped conducting polymers can usually be described by model considering small conducting island separated by resistive barriers. This barrier have been suggested to be segments of un-doped or weakly doped polymers. The Sheng model [35] is found to be appropriate to explain the charge transport mechanism in highly doped conducting polymers. In this model the process of charge transport takes place due to the tunnelling enhanced by thermal fluctuation at higher temperature through the barrier. The temperature dependence of conductivity, according to Sheng's model is given by,

$$\sigma = \sigma_o exp\left[-\frac{T_o}{T_1 + T}\right] \tag{2.4}$$

Where $\sigma_o$ and $T_o$, and $T_1$ are constants to be determined by the geometry of the barrier and the size of the conducting islands.

# Chapter 3

# Electrical Properties of Metal Semiconductor ( MS ) Contacts

The electrical properties of metal semiconductor ( MS ) contacts is determine by the work function of the metals and the semiconductors, where work function is the difference in energy between the Fermi level and the vacuum level. Based on the work function of the metals and semiconductors; the contact may be either ohmic or rectifying contact ( Schottky barrier diodes ). Both type of contacts play an important role in all kinds of solid-state devices. For examples, ohmic contacts are necessary to avoid resistance loss for almost all kinds of devices made of semiconductors [36]. Rectifying contacts are desirable for photovoltaic cells, field effect transistor, and numerous other semiconductor devices.

## 3.1 Models of a Simple Diode Made of Donor-Accepter Blend Sandwich Between Two Metals Electrodes

When a metal is making intimate contacts with a semiconductor, at equilibrium, the fermi level in two materials will coincides. If the work function of the metal is higher than the LUMO level of semiconducting polymer, an interface barrier $\varphi_b$ for electrons

will be formed.

Conjugated polymer thin film (< 100nm) sandwiched between two electrodes are usually described using a metal-insulator-metal ( MIM ) model [37]. Figure 3.1(a) represents the energetic diagrams of a bulk-heterojunction solar cell in open circuit condition. No electric field present within the device. Fig.3.1(b) shows the short circuit condition: the Fermi level of the two electrodes align themselves and a built-in-field appears in the bulk, resulting a constant slope for the HOMO and LUMO levels of the donor and acceptor.

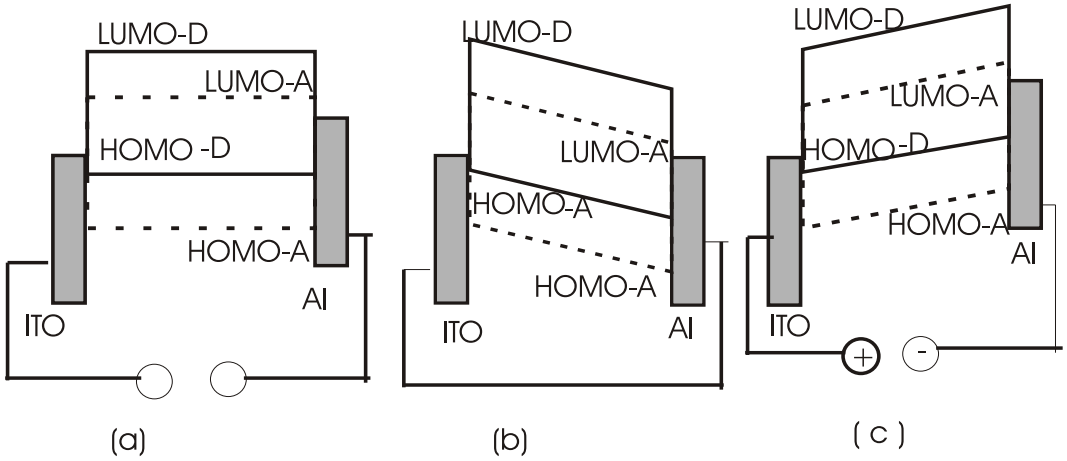


Figure 3.1: Diode made of a donor-acceptor blend sandwich between ITO and Al. (a) open circuit condition. (b) short circuit condition. (c) forward biased

.

When the devices is forward biased (ITO [anode] is connected to positive and Al [cathode] is connected to the negative terminal ) as in fig.3.1(c), electrons can be injected from cathode to LUMO level of acceptor and holes from from anode to HOMO of the donor. The effective field in the devices will ensure the drift of electrons

from cathode to anode and hole from anode to cathode. Actually, the efficiency of charge injection is driven by the energetic mismatch ($\varphi_b$) between the Fermi levels of the electrodes and the level of the band in which the charges are to be injected. If the contact is ohmic ($\varphi_b = 0$ ), the injection is mostly space charge limited [38]; the electrode supply more charge carriers per unit time than the organic semiconductor can transport; space charges appears in the vicinity of the electrodes due to the low mobilities. On the other hands, if $\varphi_b$ is important, the injection is limited by thermally assisted hopping from the Fermi level of the electrode into localized states of the semiconductor [39]. These states are usually described as belonging to Gaussian density of states broadened by energetic disorder [40].

## 3.2 Space Charge Limited Current

Space charge limited current depends on the thickness of the active layer. The space charge limited dark current conduction occurs when the contacting electrodes are capable of injecting either electrons into the conduction band or holes into the valence band of a semiconductor or an insulator, and when the initial rate of such carrier injection is higher than the rate of recombination, so that the injected carriers will form a space charge to limit the current flow.

The space-charge-limited current ( SCLC ) in a materials containing a trap distribution whose concentration decreasing exponentially inside the band gap, was investigated by Lampert and Mark [41]. They suggested that a complete current-voltage I-V curve for SCLC with an exponential distribution of traps is composed of regions governed by ohm's law ( $J \propto V$), trapped-charge-limited region ( $J \propto V^m$, $m \geq 3$ ) and Child's law region ( $J \propto V^2$). Except in ohmic region, electrical conduction is space charge limited in any case. At low voltages, electrical conduction is ohmic and the current density is described by [42].

$$J = qn\mu\frac{V}{d} \tag{3.1}$$

where q is the electronic charge, n is the free charge carriers density, $\mu$ is the carrier mobility, V is the applied voltage, and d is the film thickness.

As the bias voltage increases in the samples that have continuous trap distribution in energy, the current dependence density on the voltage is found to be [42]

$$J \propto \frac{V^m}{d^{2m-1}} \tag{3.2}$$

where m = l + 1, l $\geq$ 2 (l = $T_C$/T, $T_C$ is the characteristics temperature of the traps, T is the absolute temperature ). After this trapped charge limited current, i.e., at sufficiently high injection voltages, the traps are completely filled and do no longer influence the transport of charge carriers. The current in this case has the same behavior as a trap-free charge-limited current and is given by

$$J = \frac{9}{8}\epsilon_o\epsilon_r\frac{V^2}{d^3} \tag{3.3}$$

Here, $\epsilon_r$ and $\epsilon_o$ are relativity and free space permittivity, respectively.

Recently J.C. Jain et al. reported that the dark J-V characteristics of PPV :PCBM blends behaves like a single component polymer and fit the space charge limited conduction theory with Gaussian distribution of traps [43]. Moreover, it is demonstrated that the dark current increases with PCBM concentration. It has been indicated that this increases is due to a large electron mobility in PCBM.

## 3.3 Impedance Spectroscopy

Impedance spectroscopy is a powerfull method of characterizing many of the electrical properties of interfaces of various substance with electrically conducting materials. There are various types of electrical responses which are used in impedance spectroscopy, out of which, we focus only on the technique that enables us to measure impedance directly as a function of frequency and applied voltage.

The general approach is to apply an electrical stimulus such as voltage or current to the device under test ( DUT ). Suppose that a voltage signal $V(t) = V_m(t)\sin(\omega t)$, with a frequency $\omega = 2\pi f$, is applied to the DUT and the resulting response of current $i(t) = I_m \sin(\omega t + \theta)$ is measured, where $\theta$ is the phase difference between the voltage and the current. The conventional impedance is defined as $Z(\omega) = V(t)/i(t)$, with $\theta = \theta(\omega)$. In an orthogonal system, its magnitude and direction can be obtained from the relation Z = Z' + j Z", where $j = \sqrt{-1} = exp(\pi/2)$.

The real and imaginary part of the impedance are recorded as a function of frequency and plotted on the complex plane. The real part is plotted along the x-axis and the negative of the imaginary along the y-axis. Ideally the imaginary part of the impedance is zero at frequency, $\omega = 0$ and $\omega$ approach $\infty$ [44]. This plot from a semicircle with the center on the real axis.

One of the most attractive features of impedance spectroscopy lies in its applicability and on the studies of the direct correlation between the response of a real system and an idealized model circuit composed of discrete electrical components[45]. In modelling studies one seeks to match experimental impedance with an equivalent circuit composed of ideal resistors and capacitors. Consider RC circuit shown in Fig.

3.2(a)

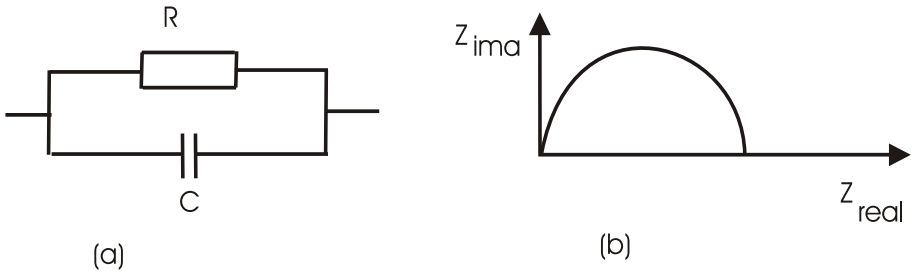


Figure 3.2: Parallel RC circuit(a) and its Cole-Cole plot

.

The impedance for the above RC circuit is given by

$$Z = \frac{R}{1 + j\omega RC} \tag{3.4}$$

normalizing this

$$Z = \frac{R}{1 + \omega^2 R^2 C^2} - j\frac{\omega R^2 C}{1 + \omega^2 R^2 C^2} \tag{3.5}$$

Where j is the imaginary number and $\omega$ is the frequency. Thus from equation ( 3.5 ) the real and imaginary parts are separated as:

$$Re(Z) = \frac{R}{1 + \omega^2 R^2 C^2} \tag{3.6}$$

and

$$Im(Z) = \frac{\omega R^2 C}{1 + \omega^2 R^2 C^2} \tag{3.7}$$

Taking the derivatives of Im(Z) with respect to angular frequency we get [45]

$$\frac{d(Im(Z))}{d\omega} = CR^2 \frac{(1 - \omega^2 R^2 C^2)}{(1 + \omega^2 R^2 C^2)^2} \tag{3.8}$$

Equation (3.8) becomes zero when $\omega = \frac{1}{RC}$. By combining equation (3.7) and (3.8), we get

$$Im(Z)_{max} = \frac{R}{2} \tag{3.9}$$

Thus, using equation (3.9) we can calculate the unknown resistance directly from $\mathrm{Im(Z)}_{max}$. The Cole-Cole [46] plot of this circuit, in its ideal form, will be a semi-circle whose center lies on the Re(Z) axis, Fig. 3.2(b). If there is a contact resistance $\mathrm{R}_C$ in series with the RC parallel circuit shown Fig. 3.3(a), the impedance will be given by

$$Z = R_C + \frac{R}{1 + j\omega RC} \tag{3.10}$$

Whose Cole-Cole plot is depicted in Fig. 3.3(b)

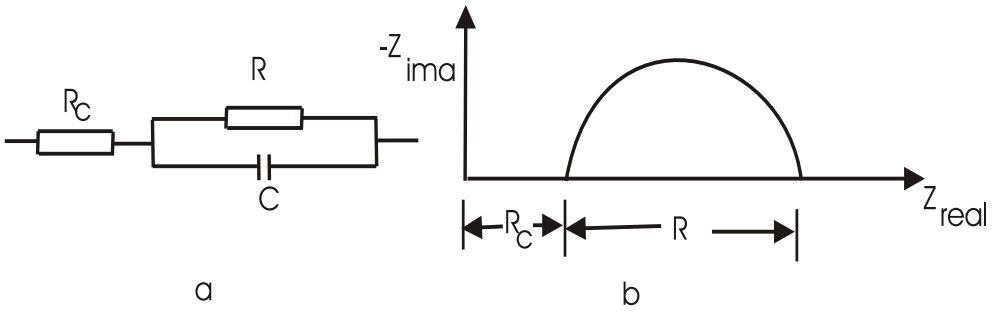


Figure 3.3: The circuit show that a contact resistance $\mathrm{R}_C$ connected in series with parallel RC circuit (a) and its Cole-Cole plot (b).

Note that the circuit model represented by Fig. 3.3 is an equivalent circuit model for a metal-semiconductor junction in which the depletion account for the observed capacitance and resistance. $\mathrm{R}_C$ accounts for the observed contact resistance at infinite frequency [47].

# Chapter 4

# Organic Solar Cells

For solar cells designed as schottky diodes, the charge separation is due to the band bending in the MS interface. Here the light absorbed in the polymer an exciton is generated. An exciton is a bound electron-hole pair. Since the binding energy of exciton [48,49] is high( 0.1-1eV ), the approximation of free carriers, as it is done for inorganic materials, is no longer valid for organic materials. The diffusion length of exciton is measured to be about 10nm[12-14]. Only carriers generated close to the Schottky junction are split into free carriers and contribute to the photo-generated current and thus, early polymer solar cells based on single layer show low power conversion efficiency.

Polymers solar cell based on a combination of donor and acceptor materials, show a dramatic increase in efficiency [50,51]. In such device photo-generation of charge carriers occurs manly by photoinduced charge transfer at a donor-acceptor interface. Most of the time the donor is the polymer. And as acceptor a $C_{60}$ or a $C_{60}$ derivatives is used. Solar cells consisting of a bilayer of donor and acceptor materials have a single D-A interface across which charge transfer takes places. Only exciton created with the diffusion length to the interface can reach the electrode [52]. This lead to the lose of photon absorbed further away from interface and consequential to low quantum

efficiency.

This limitation has been overcome by the use of a bulk-heterojunction, which is the most efficient polymer solar cells to date. Bulk-heterojunction solar cells are nanoscopically phase-separated blend of an electron donating and electron accepting materials in the active layer. This leads to donor and acceptor domains, separated by a large interfacial area compared to the bilayer. In a bulk-heterojunction, exciton have to diffuse a much shorter distance to interface and the generation takes places throughout the bulk, leading to higher charge photo-generation efficiency.

## 4.1 Bulk-heterojunction Solar Cells

Under the assumption that charge generation and separation is uniform all over the bulk, the blend of polymeric p-type semiconductor with a molecular n-type semiconductor on a nm scale is thought of be built up by one semiconductor with the conduction band given by the n-type semiconductor and valence band given by the p-type semiconductor.

The photon to electron conversion consists of several consecutive steps, which will be explained with the design and type of organic bulk-heterojunction. These process are photon absorption and generation of charge, charge separation, charge transport and collection.

The first step in the photon to electron conversion is the absorption of light. In bulk-heterojunction both materials have different absorption spectra. Here we consider the polymer a photoactive part of the blend, that consists of the electron acceptor. Upon the absorption of photons with an energy greater than the band gap $E_g$, excitons are formed. Photons with energy smaller than the band gap will not be

absorbed and will not lead to charge generation.

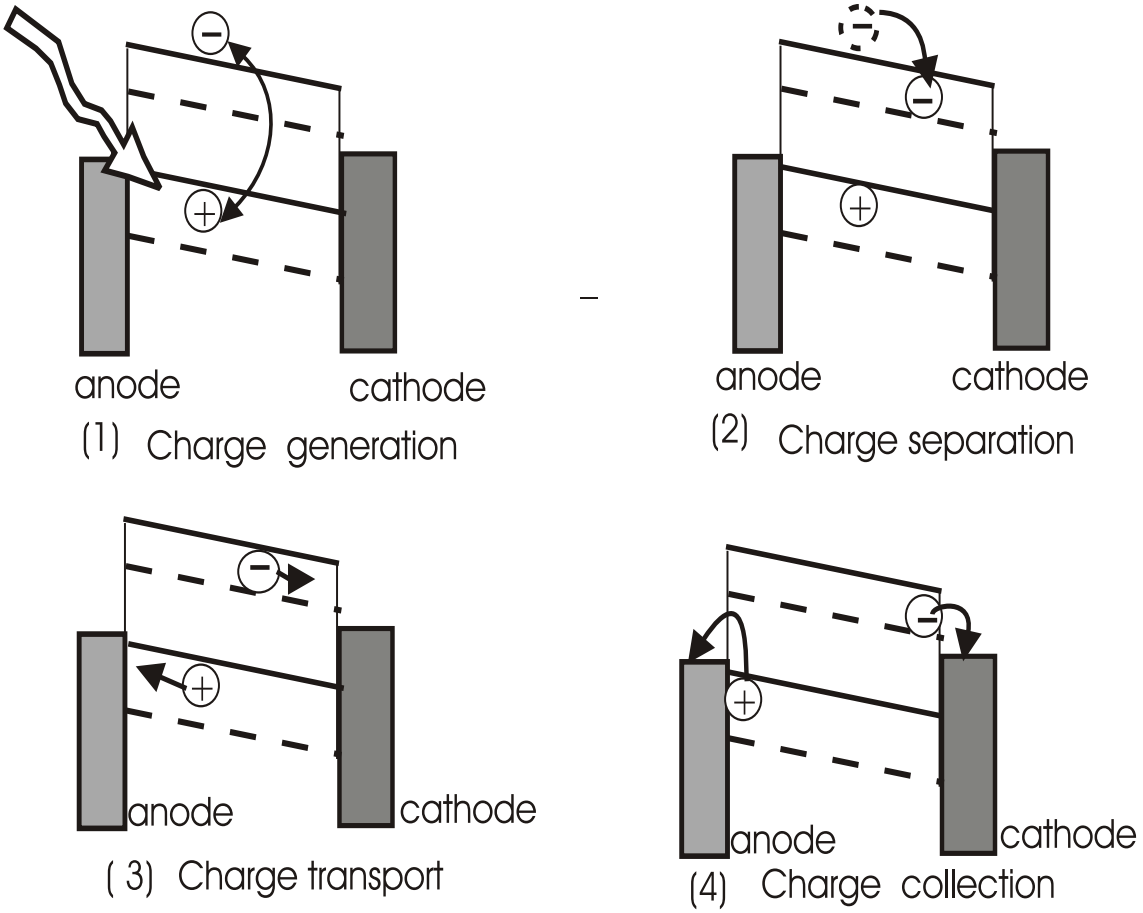


Figure 4.1: Schematic band diagram of a bulk heterojunction . The number refer to the operation processes explained in the text. The dashed line represents the energy levels of the acceptor, while the full lines indicates the energy level of the donor in photovoltaic cell.

Excitons are bound electron-hole pairs. For organic materials exciton binding energy is relatively higher [48,49], and therefore the approximation of free carriers, which is normally done for inorganic materials can not be done for organic materials. Since the binding energy of exciton is high, its diffusion length is the order of 10nm

[12-14]. As the bulk-heterojunction form a morphology with phase-separated in the nm scale, which is within the exciton diffusion length, the charge separation at the interface is efficient. On this interface the light induced charge transfer takes place [14], and the electron is transferred from the polymer to the electron acceptor, hence, hole remains on the donor polymer. This charge separation is due to an energy difference of the HOMO level of the polymer( donor) and LUMO the electron acceptor. This forward electron transfer was observed within 45fs [16], that is much faster than any computing relaxation process. Therefore, its efficiency is about 100 per cent. With this step the exciton is separated into a free hole on the polymer and a free electron on the acceptor.

The transport in organic materials is supposed to be by hopping or influenced by trapping and trap-release. The parameters of these transport mechanisms are influencing the mobilities of the carriers [53]. The deriving force for the charge carriers may be either diffusion or drift or a combination of both.

For efficient charge collection, both at the positive and negative electrodes must form ohmic contacts with the donor and acceptor networks, respectively. If this is not the case, charge collection would be limited depending on the nature of potential barrier build up at the contacts.

## 4.2 Fill factor and power conversion efficiency

In order to investigate the photovoltaic performance of a cell, as well as its electric behavior, the current density versus voltage ( J-V ) curve in the dark and illumination are considered. Figure 4.2 show a typical J-V curve of a PV device in the dark ( dashed line ) and under illumination ( solid line ).

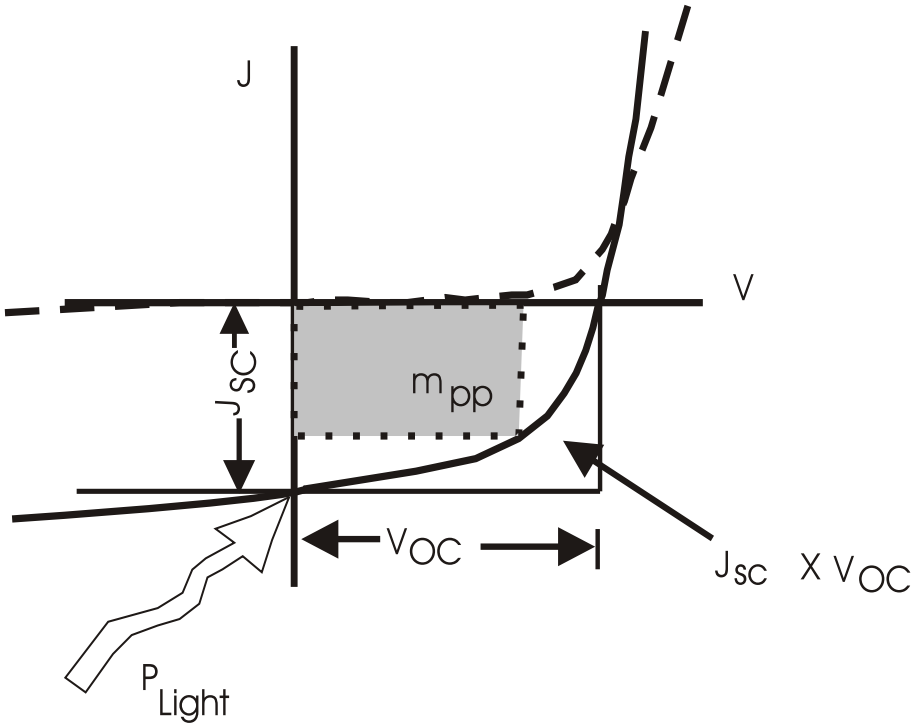


Figure 4.2: Typical J-V characteristics of organic photovoltaic cell in the dark (dashed line) and illumination (solid line) condition The maximum out put power ($M_{PP}$) is given by the shaded rectangle

Under illumination the photo-generated current density is added to the dark J-V curve. The photo-generated current under condition V=0V bias voltage is the short current density, $J_{SC}$. The intercept of the illuminated J-V curve with x-axis is the open circuit voltage, $V_{OC}$. At $V_{OC}$ the photo-generated current compensates the dark current and therefore the total current is zero.

For ideal solar cell, the J-V curve would be perpendicular and forming a rectangle together with the x-axis and y-axis. The maximum power would be the product of the $J_{SC}$ with $V_{OC}$, as depicted in figure 4.2. In reality the J-V curve deviates

from this ideal behavior and therefore the maximum power is less than this product. The maximum power of a real solar cell is determined by multiplying the measured current with each applied voltage and taking the maximum of the product in the fourth quadrant. The maximum power out put is denoted by $M_{PP}$ as depicted by the shaded region in Fig. 4.2. A measure of the fill factor of the solar cell is the ratio of $M_{PP}$ to the ideal power given by the product of short circuit current density and open circuit voltage is and given by [54].

$$FF = \frac{M_{PP}}{J_{SC} * V_{OC}} \tag{4.1}$$

The power conversion efficiency is the ratio of the maximum power extracted from the solar cell to the incident light power and can be expressed with the the $J_{SC}$, $V_{OC}$, and FF as

$$\eta = \frac{M_{PP}}{P_{in}} = \left[\frac{J_{SC} * V_{OC}}{P_{in}}\right] FF \tag{4.2}$$

Equation 4.2 shows that in order to increases power conversion efficiency, for the same incident light power $P_{in}$, either $V_{OC}$, $J_{SC}$, and $FF$ (or all) need to increased.

The origin of open circuit voltage, is a matter of controversial discussion. The upper limit of open circuit voltage is the difference between the conduction band edge of acceptor to the valence band edge of the donor. The quasi Fermi levels can split up to these bands and determined the open circuit voltage. Limitation arise due to contacts. In the model of a metal-insulator-metal ( MIM ) diode [55] the open circuit voltage is the difference of the work function of the electrodes. Alternatively,

the open circuit voltage is given by the the difference of LUMO of $C_{60}$-derivatives and the work function of semi-transparent electrodes. This takes in to account, the fullerene pins the Fermi level of the metal. If the valence band of the p-material is above the work function of the semitransparent electrodes the open circuit voltage may be reduced to the difference of the conduction band edge of $C_{60}$-derivatives to the valence band edge of p-materials [56,57].

The short circuit current is determined by the the amount of absorbed light and the internal conversion efficiency. The maximum gain for the net photocurrent may be achieved by applying materials with a lower optical band gap, allowing absorption on a broader spectral range.

# Chapter 5

# Experimental

## 5.1 Absorption Spectrum Measurement

For optical absorption spectra of pure APFO green-6 and blends of APFO green-6 and PCBM ( 1:2 by weight ratio), chloroform based solutions with concentration of 5mg/ml were prepared and spin coated on a glass substrates at a speed of 700rpm. The optical absorption spectra were recorded using a Perkin Elmer Lambeda 9 spectrophotometer and analyzed (see Fig. 6.1 and 6.2).

## 5.2 Device Preparation

Organic thin film PV device is prepared in a sandwich by creating different layers materials on the glass substrate. We used commercially available indium tin oxide ( ITO ) coated glass as a substrate, the glass was cut into pieces of area of about $3cm^2$. About half ITO covered by photoresist and the exposed part of ITO was etched out with a mixture of concentrated hydrochloric acid, nitric acid and water with volume ratio of 48:4:48 respectively. Here the photoresist is used to prevent the part ITO area against the etching acid. After removing the photoresist with acetone the ITO-glass substrate was successively cleaned with ethanol and distilled water.

On ITO-glass substrate, the PEDOT-PSS [poly(3,4ethylenedioxy thiophene)-poly (styrenesulfonate)] (Baytron-bayer AG) was spin coated at speed of 3000rpm. PEDOT-PSS was then dried at $80^o$ for 5min. PEDOT-PSS is used to smoothen the surface of ITO and, hence avoid possible short circuit due to the spiky roughness of the surface. PEDOT-PSS is known as a p-type semiconductor, a good hole transport materials, and assures a better hole collection from the active layer onto the ITO electrode. After that the active bulk-hetero junction layer was prepared by spin coating film of composite of APFO geen-6:PCBM (1:2 weight ratio) on the tope of the dry PEDOT-PSS layer. The spinner speed was 700rpm and the solution was warm up to $60^o$c for at least 20min. For top electrode, the deposition of Al is done by thermal evaporation at a pressure of $7.5\text{x}10^{-6}$mbr using Edwards Auto 306 vacuum evaporator. The cell preparation process is done in ambient condition. The device formed through all the above process has an active area of about $0.045\text{cm}^2$ see Fig. 5.1.

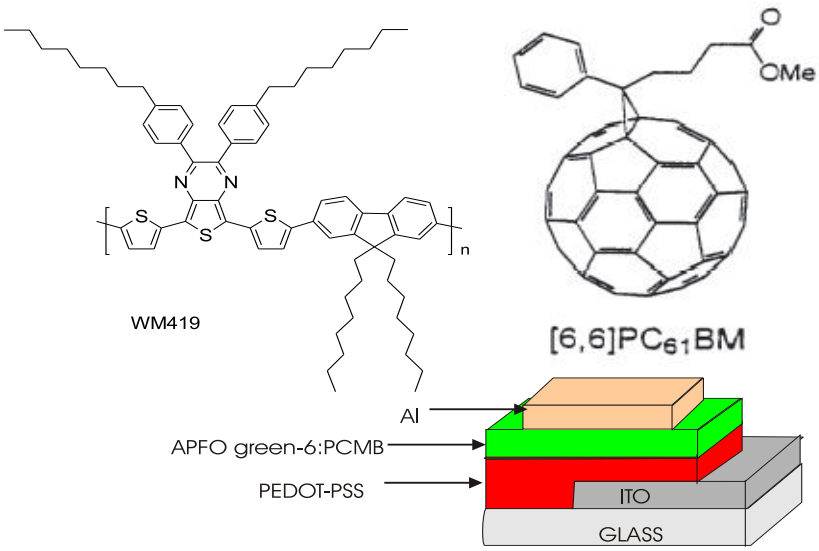


Figure 5.1: Schematics diagram of the device configuration and molecular structure of the materials used.

## 5.3 Device Characterization

The device was characterized by the I-V measurement both under dark and illumination as well as impedance spectroscopy measurements. The diode is forward biased when the Al electrode is connected to the a negative terminal.

### 5.3.1 I-V Measurement

The I-V characteristics both in the dark and under illumination were measured by computer interfaced HP Pico-Ampere meter ( model 4140B). For the dark I-V measurement, the device was placed in side an HP-test fixture (model 16055A) which is interfaced with the meter. The I-V measurement under illumination was carried out by mounting the sample in a sample holder in side a metal box having 3cm diameter opening for light entrance. The device was illuminated through ITO side with white light intensity of 80mW/cm$^2$. The curve was recorded by scanning the applied voltage between -1.2V to +1.2V and -2V to +2V, for under illumination and under dark,respectively, and recording data points in 0.05V steps.

### 5.3.2 Impedance Spectroscopy

The impedance spectroscopy as a function of frequency and biased voltage of the sandwich structure was measured using an HP 4192A LF Impedance analyzer with an HP 16047A test fixture. The complex impedance of the device was measured at a frequencies ranging from 500Hz to 50KHz for bias voltage ranging from -3V to3V in steps of 1V. For every bias voltage, a sinusoidal oscillating voltage of $V_{rms}$=50mV was used. The Cole-Cole plot of the device is given in Fig. 6.6

# Chapter 6

# Result and Discussion

## 6.1 Absorption Spectrum

The optical absorption of APFO green-6 is shown in Fig. 6.1. The onset optical absorption occurs at wavelength near 786nm. Using the relation $E_g = \frac{hc}{\lambda}$, the band gap of APFO-Green 6 is calculated to be 1.58eV, which is in the range of energy gap as that of inorganic semiconductors.

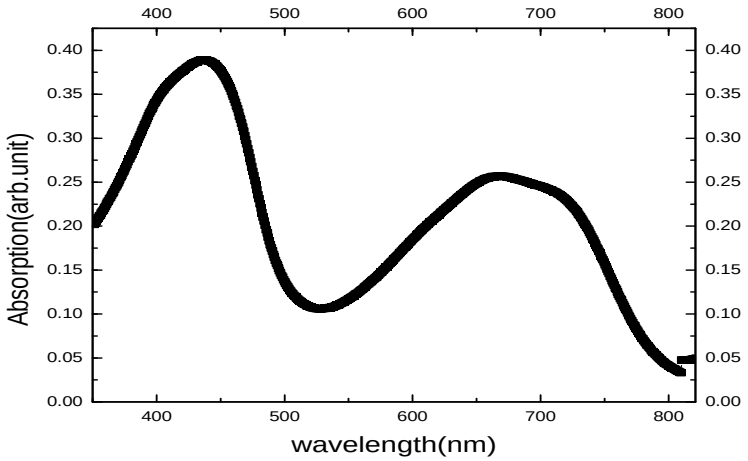


Figure 6.1: Absorption spectrum of APFO-Green-6

The optical absorption spectra for the blend and for pure polymer are presented in Figure 6.2. Normalization to the peak value is done for the purpose of comparison. No significant difference was found on comparing corresponding peaks in the spectra for pure polymer and the blend, which suggest that there is no charge transfer the APFO green-6 to PCPM. That means there is no ground state doping of APFO green-6 by PCBM.

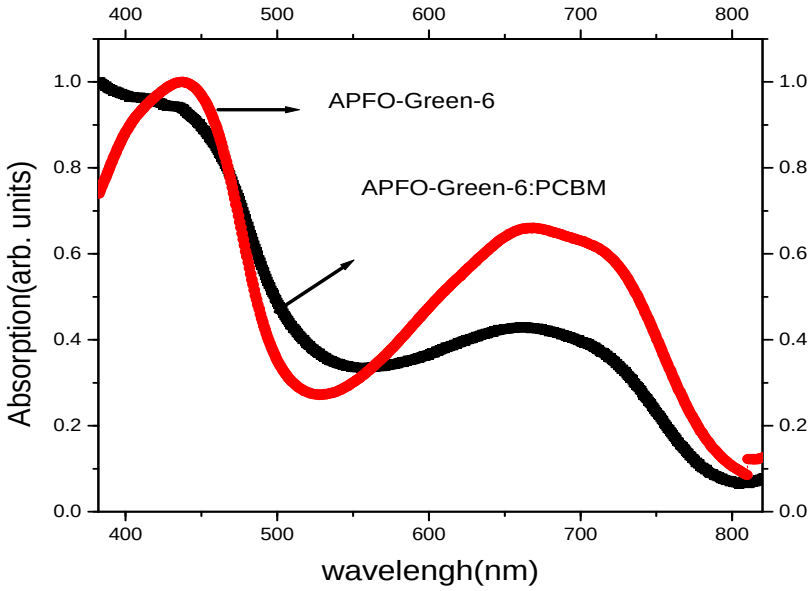


Figure 6.2: Optical absorption of APFO green-6 and blend of APFO green-6 and PCBM (1:2 weight ratio)

## 6.2 Dark J-V Characteristics

Figure 6.3 shows that dark current density of our cell as a function of applied voltage at room temperature. The J-V characteristics are non-linear and the rectification ratio at $\pm$ 2V is 6273.

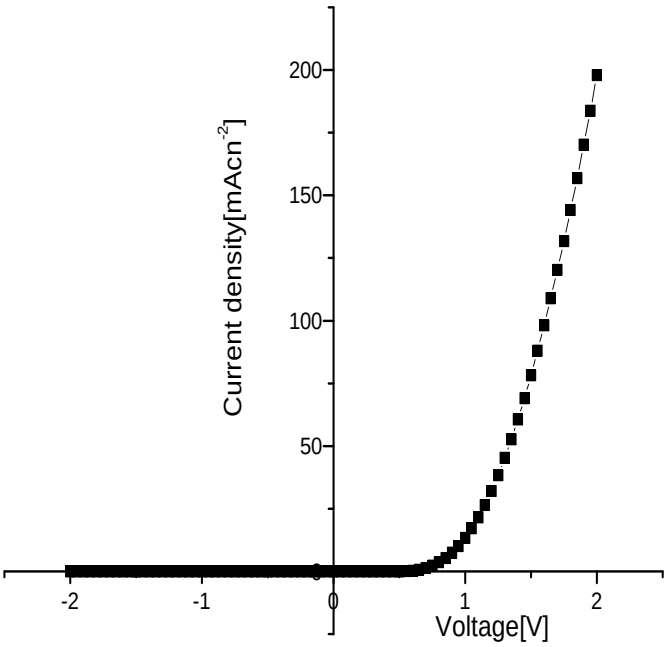


Figure 6.3: J-V characteristics under dark.

Figure 6.4 shows the plot of ln J versus ln V only in forward direction. The analysis of this curve provides important information about the charge transport phenomena of our device. At lower voltages, the ln J versus ln V plot of our device yields a relation ship of J $\propto$ V, which suggests that the current is ohmic. At intermediate voltages the current density varies as $V^m$ where m is greater than two. This behavior indicates that the current is trap controlled space charge limited [45,58,59].

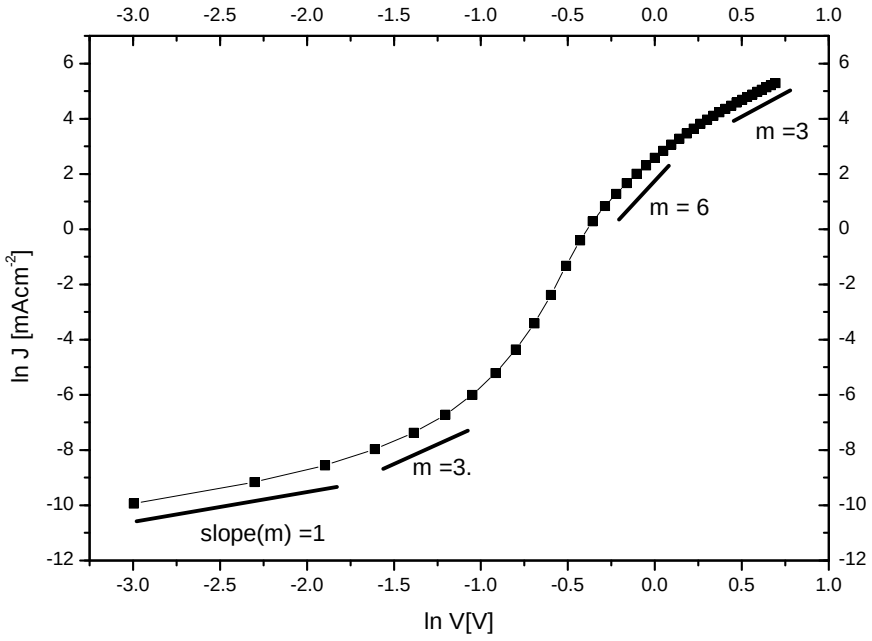


Figure 6.4: Plot of ln J-ln V in forward direction.

It is shown that as the voltages increases further the rate of increase of current with voltage decreases. This happens because now most of the traps are filled and contribution of free carries to the electric filled becomes appreciable. Now, the current approaches the trap free space charge limited region with $V^2$ dependence [58]. However, that relationship has not been observed within our measurement range.

Recently J.C. Jain et al.[43] show that the dark current density of ITO/PEDOT-PSS/PPV :PCBM/Al at low voltages is not due to the excitation of carriers from HOMO of donor to LUNO of acceptor because this process requires much larger energy of activation ( $E_a$ = 80meV). The ohmic behavior at low voltages seems to be

due to background impurities [60]. The origin and nature of these impurities in the blends are not known.

Between -0.2V and +0.2V the logarithmically plotted dark current ( see Fig.6.5 ) is nearly symmetric to the 0V for the positive and negative applied voltages. Such a symmetry can be explained by the contribution of a small shunt resistance to the dark current. Small shunt manifests as 'ohmic' behavior in low current regime of a diode [61].

## 6.3 J-V Characteristics Under Illumination

Figure 6.4 (a), (b) shows the linear and semi-logarithmic plot of J-V characteristics of cell ITO/PEDOT-PSS/APFO green-6:PCBM/Al ( 1:2 weight ratio ) in the dark and under white light illumination ( 80mW/cm$^2$ ). The open circuit voltage $V_{OC}$, short circuit current density $J_{SC}$, the fill factor FF and power conversion efficiency $\eta$ of the cell under white light illumination ( 80mW/cm$^2$ ) are 547mV, 0.31mA/cm$^2$, 0.5 and 0.107 %, respectively.

The PV cell shows photo-conducting property. At +1.2V a photocurrent of 47mA/cm$^2$ is observed, while the dark current is measured with 32mA/cm$^2$. The difference between the photocurrent density and the dark current density at +1.2V is 15mA/cm$^2$. The observed Photoconductivity indicates that in this cell bipolar charge transport is restricted [61].

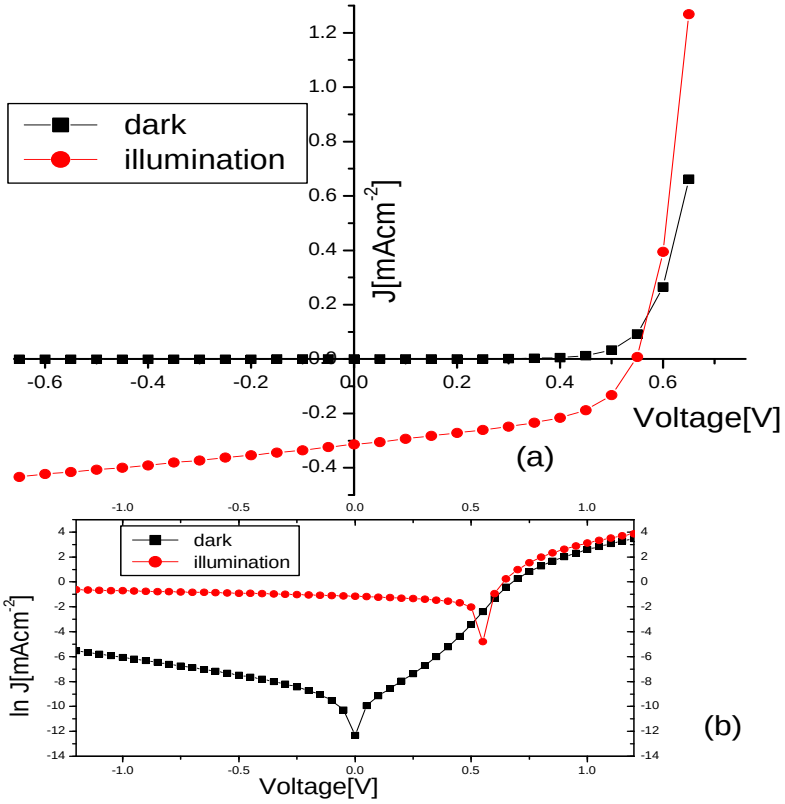


Figure 6.5: J-V characteristics of our cell (a) linear (b)semilogarithimic scale in dark and under illumination.

## 6.4 Impedance Spectroscopy

Fig. 6.6 shows the impedance spectroscopy of our device as a function of frequency and applied voltage. The filled points are the measured coordinates of the real and imaginary part of the impedance. The impedance spectra consists of single semicircle whose diameter correspond to the resistance of the depletion region for corresponding bias voltage. These semicircle is bias dependent. The smaller bias voltages give semicircle with larger diameter. This is consistent with J-V curves of our device (see

Fig. 6.3).

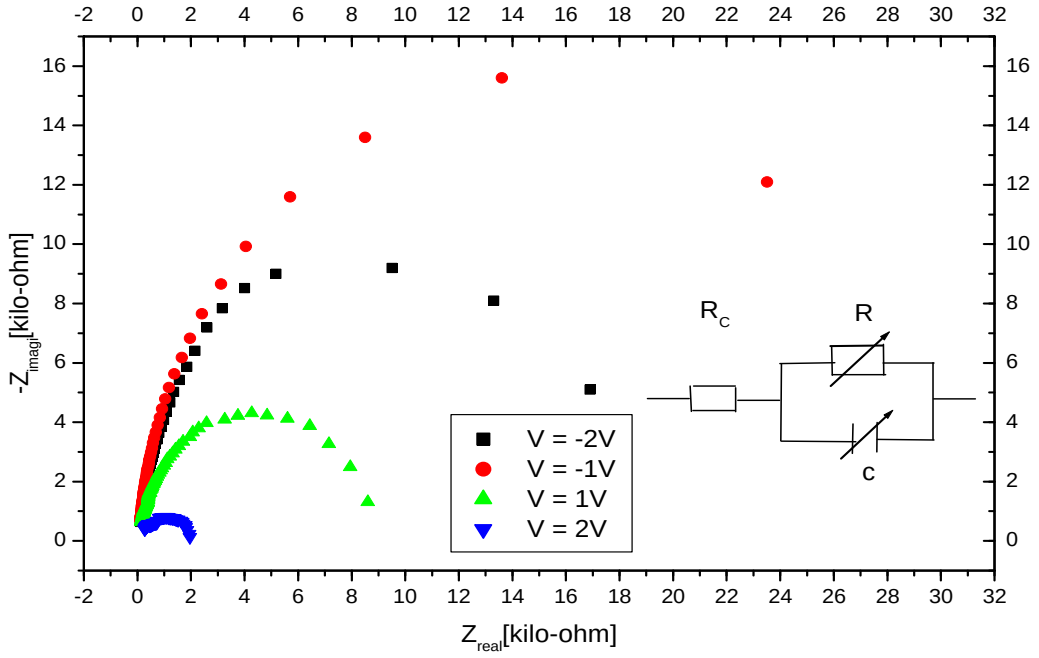


Figure 6.6: Cole-Cole plot of our device

.

The device is described by using the metal-insulator-metal picture. This means that the device is thought of be built of one semiconductor with the LUMO of the acceptor and HOMO of the donor as conduction band and valence band, respectively.

From the work function, it is expected that the work function of PEDOT-PSS ($\phi_{PEDOT-PSS}$ = 5.2eV [62] and HOMO of APFO Green-6 (= 5.1eV) form an ohomic contact for hole injection to HOMO level of the APFO Green-6, The work function of Al ($\phi_{Al}$ = 4.3eV) do not much with the LUMO level of PCBM ( = 3.7eV ), which

result in interface barrier of $\varphi_b = 0.6$eV for the electron to inject to the LUMO level of the PCBM. Therefore, there is a single barrier at Al/semiconductor interface.

An ideal Cole-Cole plot of the complex impedance is a semicircle with its center, the zero frequency and the infinite frequency intercept on the $Z_{real}$ [44]. This single semicircle support a model where there is a single barrier at Al/semiconductor interface. There is no evidence for a partially or completely overlapping of the second semicircle due to a barrier at the other electrode. Usually the zero frequency real impedance is obtained by extrapolating. The contact resistance, $R_C$, is the distance from the origin to the intersecting of the semicircle with the real axis of the impedance plot corresponding to the highest frequency. Thus we model our device ITI/PEDOT-PSS/APFO green-6:PCMB/Al by one parallel RC circuit in series with the contact resistance as indicated in the inset of fig. 6.6. The relation $Z_{imagi}$ - $[\omega C]^{-1}$ is used to estimate the value of capacitance. The parameter obtained from the Cole-Cole plot are listed in table 6.1.

Table 6.1: Parameters obtained from Fig. 6.6

| $V_b(V)$ | $R_C$ $\Omega$ | R K$\Omega$ | C(nF/cm$^2$) |
|---|---|---|---|
| 2 | 30 | 2 | 8.3 |
| 1 | 30 | 8.62 | 6.87 |
| -1 | 30 | 30 | 5.1 |
| -2 | 30 | 20 | 5.58 |

.

# Conclusion

In this work bulk-heterojunction PV cell was fabricated which is composites of APFO green-6 and PCBM (1:2 wt ratio) in a sandwich structure of ITO/PEDOT-PSS/APFO Green-6: PCBM/Al. The device was characterized by J-V measurements under dark and illumination as well as by Impedance spectroscopy. The energy gap of APFO Green-6 was estimated to be 1.58eV from optical absorption spectrum. The Optical absorption spectrum of a blend show that there is no significant difference on compering peak in the spectra for pure APFO Green-6 and the blend, which suggest that there is no charge transfer from APFO Green-6 to PCBM. The dark J-V curve of our device manifests the properties of trap-controlled space charged limited charge transport i,e., J $\sim$ V$^m$, m $>$ two. However, at low voltages, the current is nearly proportional to the voltages, which suggest that the current is ohmic. From J-V curve under 80mA/cm$^2$ white light intensity, $V_{OC}$ = 547mV, $J_{SC}$ = 0.314mA/cm$^2$, FF = 0.5 and $\eta = 0.107$ % were determined. The complex impedance curve at different bias voltages shows the impedance of the bulk at reverse bias voltages is larger than the impedance of the corresponding forward bias. This is consistent with rectification behavior observed from the dark J-V characteristics. From the impedance spectroscopy a contact resistance $R_C$ = 30 $\Omega$ is obtained and various bulk resistance as given in Table 6.1

# Bibliography


[1] A.J. Heeger, *Journal of Physical Chemistry* B **105** (2001) 8475.

[2] C.K Chiang, C.R. Jr. Fincher, Y.W. Park, A.J. Heeger, H. Shirakawa, E.J. Louis, S.C. Gau, A.G. MacMiarmid, *Phys. Rev. Lett.*, **39** (1977) 1098.

[3] http:/www.nobel.se/announcement/2000/cheminfoen.html

[4] G. Yu, A.J Heeger, *Journal of Applied Physics* **78** (1995) 4510.

[5] H. Koezzuka, A. Tsumura, *Synthetic Metals* **28** (1983) C753.

[6] M. Berggen, O, Inganäs, G. Gustafsson, J.C Carlberg, J. Rasmusson, M.R. Andersson, T. Hjertberg, O. Wennerstöm, *Nature* **372** (1994) 187.

[7] D.M Chapin, C.S. Fuller and G.L. Pearson, *Journal of Applied Physics*, **25** (1954) 676.

[8] M.A. Green, K. Emery, D.L. King, S. Igari, W. Warta, *Prodress in Photovoltaics*, **13** (2005) 49.

[9] A. Geotzberger, C. Hebling, H.W. Schock, *Material Science and Engneering Reports* **40** (2003) 1.

[10] G.A. Chamberlain: *Solar Cells* , **8** (1983)47.

[11] D. Wehrle and D. Meissner,*Adv. Mater.* **3** (1991) 129

[12] H.R. Kerp, H. Donker, B.M. Kochorst, T.J. Schaafsma, and E.E Van Faasen, *Chem. Phys. Lett.*,**298**(1998)302.

[13] A. Haugernerder, M. Neges, C. Kallinger, W. Spirkel, U. Lemmer, J. Feldman, U. Schertf, E. Harth, A.Gugel, and K. Mullen, *Phys. Rev.* B, **59** (1999) 15345.

[14] N.S. Sariciftci, L. Smilowitz, A.J. Heeger, and F. Wudl, *Science*, **258** (1992) 1474.

[15] A. Gadisa and B. Workalemahu, *Synthetic Metals*, **129** (2002) 179.

[16] C.J. Brabec, G. Zerza, G. Cerullo, S. De Silvestri, S. Luzzati, J.C. Hummelen. N.S. Sariciftci, *Chem. Phys. Lett.*.**340** (2001) 232.

[17] S.E. Shahaeen, C.J. Brabec, N.S. Sariciftci, F. Pandinger, T. Fromherz, J.C. Hummelen, *Appl. Phys. Lett.*, **78** (2001) 841.

[18] D. Chirvase, J. Parisi, J.C. Hummelen, V. Dyakonove, *Nanotechnology*, **16** (2004) 1317.

[19] Y. Kim, S.A. Choulis, J. Nelson, D.D.C. Bradley, S. Cook, and J.R. Durrant, *Appl. Phys. Lett.*,**78** (2005) 063502.

[20] F. Pandinger, R.S. Rittberg, N.S. Sariciftci, *Adv. Func. Mater.*, **13** (2003) 85.

[21] C.J. Brabec, *Solat Energy Materials and Solar cells*, **83** (2004) 273.

[22] T.W.G. Solomon, *Fundamentals of Organic Chemistry*, John Willey and Sons, New York, 1990.

[23] N.W. Ashcroft and N.D. Mermin, *Solid State Physics*, Holt, Rinehart and Winston, N. Y., (1976).

[24] Bantikassegn Workalemahu, Ph.D Dissertation, ISBN 91-7871-803-1, Linkoping University, Sweden, 1996.

[25] J.T. Devrees, R.P. Evrard and V.E. Van Doren, *Highly Conducting One-Dimendional Solids*, Plenum, New York, 1978.

[26] R.E. Peierls, *Quantum theory of solids*, Clarendon Press, Oxford, 1955.

[27] H. Stubb, E. Punkka, and J. Polocheimo, *Material Science and Engineering*, **10** (1983) 85.

[28] J. Tonoka and M. Tanaka, *in Handbook of conducting polymers*, vol 2, edited by T.A. Skotheim Marcel Dekker. Inc. New York and Basel, 1996 pp 856-913.

[29] Jan Przyluski, *Solid State Phenomena*,vol 13 and 14, Scien-Tech Publication Ltd, Liechtenstein, 1991.

[30] A.J. Heeger, S.K. Kiverson, J.R. Schriefter and W.P. Su, *Rev. Mod. Phys.*, **60** (1998) 782.

[31] P. Chandrasckhar, *Conducting Polymers*,Kluwer Academic Publishers, 1999.

[32] N.F. Matt and E.A. Davis, *Electronic Processes in Non-crystalline Materials* Clarendon, Oxford, 1979.

[33] E. Punkka, M.F. Ruber, J.D. Hettinger, J.S. Brooks and S.T. Hannans, *Phys. Rev.*, B **43** (1991) 9076.

[34] C.O. Yoon, M. Reghu, D. Moses and A. J. Heeger, *Phys. Rev.*, B **49** (1994) 10851.

[35] P. Sheng and J. Klafter, *Phys. Rev.*, B **27** (1983) 2583.

[36] S.M. Sze, *Physics of Semiconductor Devices*, $2^{nd}$ ed., John Wiley and Sons, New York, 1981.

[37] I.D. Patker, *J. Appl. Phys.*, **75** (1994) 1656.

[38] R.I. Frank and J.G.Simmons, *J. Appl. Phys.*, **38** (1967)832.

[39] V.I. Arkhipov, E,V. Emelianova, Y.H. Tak, and H. Basser, *J. Appl. Phys.*, **79** (1998)848.

[40] H. Basser, *Phys. Status Solidi B* ,**175** (1993) 15

[41] M.A. Lampert and P. Mark, *Current Injection into Solids*, Academic, New York, 1970.

[42] M.A. Lampert, *J. Appl. Phys.*,**103** (1956)1648.

[43] J.C. Jain, T. Aernout, A.K. Kapor, V. Kumar, Wim Greens, J. Poortmans, and R. Mertens, *Synthetic Metals*, **148** (2005) 245.

[44] T.A. Skothein, R.I. Elesenbuamber, and J.R. Reynolds, *Hand book of conducting polymer*, Marcel Dekkern Inc., (1998).

[45] Javan Mijovic and Francessco Bullucci, *Rev. Impedance Spectroscopy of Reactive Polymers*, Elsevier Science Ltd, 1996.

[46] K.S. Cole and R.H. Cole, *J. Chem. Phys.*, **9** (1941) 341.

[47] W. Bantikassegn, O. Inganas, *Thin Solid Films*, **293** (1997) 138.

[48] B.A. Gregg and M.C. Hana, *J. Appl. Phys.*, **93** (2003) 2605.

[49] M. Pope and C.E. Swenberg, *Electronic Process in Organic Crystal and Polymers*, $2^{nd}$ ed, Oxford University Press, New York, 1999.

[50] C.J. Brabec, S.E. Shaheen, C. Winder, N.S. Sariciftci, and P. Denk, *Appl. Phys. Lett.*, **80** (2002) 1288.

[51] J.J.M. Halls, and R.H. Friend, *Synthetic Metals*, **85** (1997) 1307.

[52] M. Theander, A, Yartesv, D. Zigmantas, V. Sundstrom, W. Mammo, M.R. Andersson, and O. Inganas, *Phys. Rev. B*, **60** (2000)12957.

[53] P.W.M. Blom, M.J.M. de Jong, and M.G. van Munster, *Phys. Rev.*, B **55** (1997) 656.

[54] H. Hoppe and N.S. Sariciftci, *J. Mater. Res.*, **19** (2004) 7.

[55] V.D. Mihailetch, P.W.M. Blom, J.C. Hummelen, and M.T. Rispens, *J. Appl. Phys.*, **94** (2003) 6849.

[56] S. Spiekermann, G. Smestand, J. Kowalik, L.M. Tolbert, and M. Gratzel, *Synthetic Metals*, **121** (2001) 1603.

[57] H. Frohne, S. Shahhen, J.C. Brabec, D.C. Muller, N.S. Sariciftci, and K. Meerholz, *Chem. Phys. Chem.*, **9** (2001) 795.

[58] S.C, Jain, A.K. Kapoor, W. Geens, J. Poortmans, R. Mertens, M. Willander, *J. Appl. Phys.*, **92** (2002) 3579.

[59] K.C. Kao, H. Wwang, *Electrical transport in in solids*, Pwrgamon Press, Oxford, 1981.

[60] S.C. Jain, W.Greens, A. Mehra, V. Kumar, T. Aernaus, J. Poortmans, R. Mertens, *J. Appl. Phys.*, **92** (2002) 3725.

[61] D. Gebeyehu, C.J. Brabec, F. Padinger, T. Fromherz, J.C. Hummelen, B. Badit, N.S. Saricftci, *Synthetic Metals*, **118** (2001) 1.

[62] C.J. Brabec, N.S. Sariciftci, C.J. Hummelen, *Adv. Fun. Mater.*, **11** (2001) 15.

## DECLARATION

I hereby declare that this thesis is my original work and has not been presented for a degree in any other University. All sources of material used for the thesis have been duly acknowledged.

**Name:** ***Tesfaye Mamuye***

**Signature:**_____

This thesis has been submitted for examination with my approval as university advisor.

**Name:** ***Dr. Genene Tessema***

**Signature:**_____

Addis Ababa University
Department of Physics
July, 2006.